Lattice dynamical properties of superconducting SrPt$_3$P studied via inelastic x-ray scattering and density functional perturbation theory

D. A. Zocco,[1, *] S. Krannich,[1] R. Heid,[1] K-P. Bohnen,[1] T. Wolf,[1] T. Forrest,[2] A. Bossak,[2] and F. Weber[1, †]

^{1}Institute for Solid State Physics (IFP), Karlsruhe Institute of Technology, D-76021 Karlsruhe, Germany
^{2}European Synchrotron Radiation Facility (ESRF), F-38043 Grenoble Cedex, France

We present a study of the lattice dynamical properties of superconducting SrPt$_3$P ($T_c = 8.4$ K) via high-resolution inelastic x-ray scattering (IXS) and *ab initio* calculations. Density functional perturbation theory including spin-orbit coupling (SOC) results in enhanced electron-phonon coupling (EPC) for the optic phonon modes originating from the Pt(I) atoms, with energies ~ 5 meV, resulting in a large EPC constant $\lambda \sim 2$. An overall softening of the IXS powder spectra occurs from room to low temperatures, consistent with the predicted strong EPC and with recent specific-heat experiments ($2\Delta_0/k_B T_c \sim 5$). The low-lying phonon modes observed in the experiments are approximately 1.5 meV harder than the corresponding calculated phonon branch. Moreover, we do not find any changes in the spectra upon entering the superconducting phase. We conclude that current theoretical calculations underestimate the energy of the lowest band of phonon modes indicating that the coupling of these modes to the electronic subsystem is overestimated.

The search for high-temperature superconductivity has been lately focused in materials presenting unconventional Cooper-pairing mechanisms, such as in the copper-oxide and iron-based superconductors, in which it is believed that the attractive binding force between electrons arises from magnetic exchange interactions [1]. Phonon-mediated superconductivity, however, has never left the scene, with materials like MgB$_2$ [2] or hydrogen metallic alloys, in which it has been predicted [3] and recently demonstrated in high-pressure experiments[4] that high phonon frequencies due to the light atoms having strong EPC can lead to high values of T_c. Additionally, low-frequency phonons in compounds containing heavier elements could give sizeable T_c values via enhanced EPC.

Recently, a new family of ternary platinum phosphide superconductors APt$_3$P with $A = $ La, Ca, Sr was discovered [5], presenting T_c's of 1.5, 6.6 and 8.4 K, respectively. These materials crystallize in a tetragonal antiperovskite structure (space group $P4/nmm$) similar to that of the non-centrosymmetric heavy-fermion superconductor CePt$_3$Si, although the phosphorous compounds maintain the inversion symmetry. The structure consists of alternating layers of A atoms and distorted Pt$_6$P octahedra, which leads to two different Pt lattice sites (Fig. 1(a)). For SrPt$_3$P, specific-heat [5] $C(T)$ and muon-spin rotation [6] (μSR) measurements revealed superconducting gap energies $\Delta_0 = 1.85$ and 1.55 meV and ratios $2\Delta_0/k_B T_c \sim 5.1$ and 4.3, respectively, providing evidence for very strong-coupling, fully-gapped s-wave superconductivity. Anomalous curvature of the upper critical field was interpreted as strong SOC inherent to the $5d$ Pt orbitals [5] but also as arising from a two-band superconducting state with equal gaps but differing values of the coherence lengths [6].

The coupling of superconducting charge carriers to low-lying phonons in SrPt$_3$P was first inferred from a non-linear normal-state specific heat [5] and it has been later corroborated by first-principle calculations [7–10]. No indications of phonon softening were found in the calculated phonon dispersions [9], and the effect of SOC of Pt on the superconductivity was reported as negligible [8–10].

We present the first experimental study of the phonon spectrum of SrPt$_3$P, performed via high-energy-resolution IXS measurements of a high-quality powder sample. An overall softening of the spectrum at low temperatures is consistent with the strong EPC obtained from our supporting *ab initio* calculations. The experimental results suggest, however, that theoretical calculations overestimate the strength of the EPC.

Density-functional theory (DFT) calculations were performed within a mixed-basis pseudopotential (PP) framework [11, 12], within the local density approximation (LDA) in the parametrization of Perdew-Wang [13]. Norm-conserving PPs were constructed from all-electron relativistic atom calculations according to the scheme of Vanderbilt [14] and include non-linear core corrections. Spin-orbit coupling (SOC) was incorporated within the PP approach [15, 16] and treated fully self-consistently in the ground-state calculations [17]. Plane waves up to a kinetic energy of 22 Ry were augmented with local functions of s and p type at the P sites, and s, p, and d types at Sr and Pt sites. This choice of the basis set guaranteed sufficient convergence of electronic and phononic properties. Brillouin zone summations were performed with regular k-point meshes in combination with the standard smearing technique [18] employing a Gaussian broadening of 0.1 eV [19]. The results for the lattice optimizations are summarized in Fig. 1(b). Overall, our LDA calculations including SOC are in good agreement with the previously reported results, with bands near the Fermi level dominated by Pt(I) and Pt(II) $5d$-states [8–10].

Phonon and electron-phonon coupling (EPC) properties were obtained via density-functional perturbation theory (DFPT) [20, 21]. The calculated phonon dispersion $\omega(k)$ of $SrPt_3P$ and the phonon density of states (PDOS) are displayed in Figures 1(c) and (d), respectively. At high frequencies, the phonon dispersion is dominated by the vibrations of P-atoms, which determines almost entirely the PDOS. On the other hand, optic modes originating from the in-plane motion of Pt(I) atoms dominate the low-frequency part of the phonon dispersion and PDOS. The calculations show that the EPC is strongly manifested in the phonon modes with energies $\sim 5\,\mathrm{meV}$. This strong coupling is represented [22] by the relative phonon linewidth γ/ω (red vertical bars)

$$\frac{\gamma_{\mathbf{q},\lambda}}{\omega_{\mathbf{q},\lambda}} = 2\pi \sum_{\mathbf{k},\nu,\nu'} |g^{\mathbf{q},\lambda}_{\mathbf{k}+\mathbf{q},\nu';\mathbf{k},\nu}|^2 \delta(\epsilon_{\mathbf{k},\nu}-E_F)\delta(\epsilon_{\mathbf{k}+\mathbf{q},\nu'}-E_F) \quad (1)$$

where $\epsilon_{\mathbf{k},\nu}$ are the electronic energies with momentum $\mathbf{k}$ and band index ν, $g^{\mathbf{q},\lambda}_{\mathbf{k}+\mathbf{q},\nu';\mathbf{k},\nu}$ are the electron-phonon matrix elements, and E_F is the Fermi energy. The relative linewidth describes an isotropic s-wave superconductor via the Eliashberg function

$$\alpha^2 F(\omega) = \frac{1}{2\pi\hbar N(E_F)} \sum_{\mathbf{q},\lambda} \frac{\gamma_{\mathbf{q},\lambda}}{\omega_{\mathbf{q},\lambda}} \delta(\omega - \omega_{\mathbf{q},\lambda}), \quad (2)$$

where $N(E_F)$ denotes the electronic density of states per atom and spin at the Fermi energy, and from which one can estimate the average EPC constant λ:

$$\lambda = 2\int_0^\infty d\omega \frac{\alpha^2 F(\omega)}{\omega} = \frac{1}{\pi\hbar N(E_F)} \sum_{\mathbf{q},\lambda} \frac{\gamma_{\mathbf{q},\lambda}}{\omega_{\mathbf{q},\lambda}^2}. \quad (3)$$

The two functions are plotted in Fig. 1(e). Clearly, the strongly-coupled low-energy Pt(I) vibrations constitute the main contribution to $\alpha^2 F(\omega)$, resulting in the large coupling constant value $\lambda = 1.97$, and transition temperature $T_c = 9.4\,\mathrm{K}$ estimated from the solution of the full-gap equations using a Coulomb pseudopotential $\mu^* = 0.1$. For $SrPt_3P$ the strong coupling of the low-lying phonons to the electronic states is consistent with the experimental observations made by Takayama *et al.* from electrical resistivity and specific-heat measurements [5]. Contrary to previously published results [9, 10], the inclusion of SOC in our calculations is responsible for a 23% increase in the value of λ (from 1.60 to 1.97), mainly due to a shift of the low-energy phonons towards lower energies (Eq. [3]). SOC was recently included in the calculations of λ for elementary Pb, resulting in larger values that explain its strong EPC effects observed in experiments [17].

In order to test the lattice dynamical properties of $SrPt_3P$ and the possible strong electron-phonon coupling effects on the superconducting state, we performed high-energy-resolution IXS experiments. Polycrystalline powder samples were prepared via conventional solid state reaction. X-ray diffraction performed on our samples revealed powders containing more than 90% of the desired $SrPt_3P$ superconducting phase, with a $T_c = 8.5\,\mathrm{K}$
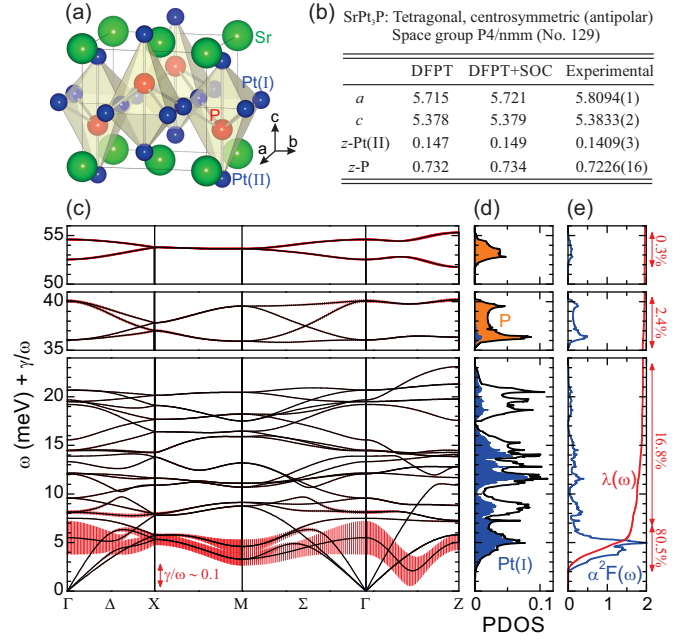

FIG. 1: (color online). (a) Crystal structure of $SrPt_3P$. Platinum atoms occupy two distinct positions, Pt(I) and (II). (b) Calculated and experimental [5] lattice parameters. (c) Calculated phonon dispersions $\omega(k)$ and relative phonon linewidths γ/ω (red vertical bars, amplified for clarity). SOC was included in the calculations (see text). (d) Calculated PDOS (black lines) vs ω. The colored regions emphasize the dominant atoms determining the dispersion at low (Pt(I), blue) and high (P, orange) energies. (e) Calculated isotropic Eliashberg function $\alpha^2 F(\omega)$ (blue line) and EPC constant $\lambda(\omega)$ (red line) vs ω. Percentages indicate the contribution of $\alpha^2 F(\omega)$ to $\lambda(\omega)$ in different energy ranges.

determined from ac-susceptibility measurements. The IXS measurements were performed at the ID28 beamline located at the European Synchrotron Radiation Facility (ESRF), between room temperature and $2.5\,\mathrm{K}$ using a continuous flow cryostat. A monochromatic incident beam with energy $E_i = 21.747\,\mathrm{keV}$ was obtained from the (11,11,11)-Bragg reflection of a silicon-crystal monochromator which operates in a backscattering geometry. The energy resolution in this experiment was $\sim 1.5\,\mathrm{meV}$ [23].

The energy scans performed for $Q = 5.7\,\text{Å}^{-1}$ at $300\,\mathrm{K}$ and $10\,\mathrm{K}$ are displayed in Fig. 2(a). Fig. 2(b) displays an example of raw data (empty circles) measured at $300\,\mathrm{K}$. The spectrum consist mainly of a strong elastic peak arising from incoherent scattering and the inelastic contribution originating from phonon scattering. Tails of Debye-Scherrer rings were largely avoided by a suitable choice of the scattering angle. The elastic peaks were fitted with a pseudo-Voight function (blue line) with 80% of Lorentzian-shape component, consistent with the spectrometer's resolution characterization. Inelastic phonon spectra (filled circles) were obtained after subtracting the elastic peaks from the total counts and were normalized with the corresponding Bose-factor. As Fig. 2(b) shows,
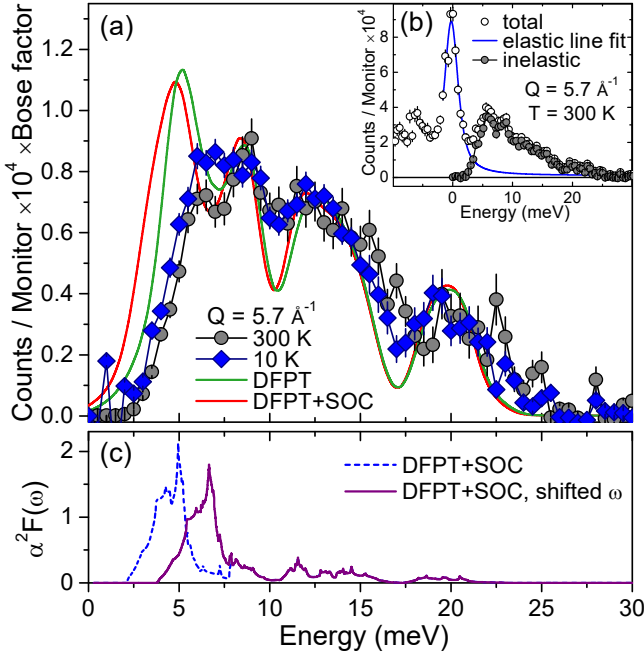
FIG. 2: (color online). (a) Inelastic data from combined energy scans at $Q = 5.7\,\text{Å}^{-1}$ obtained at $300\,\text{K}$ (circles) and $10\,\text{K}$ (diamonds). Powder-average calculations of the dynamical structure factors are shown for $Q = 5.7\,\text{Å}^{-1}$ as green (no SOC) and red (with SOC) lines. (b) A representative energy scan measured between $-10\,\text{meV}$ and $30\,\text{meV}$ (empty symbols). The inelastic phonon component (full symbols) was obtained after subtracting the fit to the incoherent-elastic peak contribution (blue line). (c) Scaling of the Eliashberg function $\alpha^2 F(\omega)$ by a shift in energy $\omega_{sh} \to \omega + 1.7\,\text{meV}$.

the low energy part of the spectra is dominated by the temperature independent elastic scattering. Therefore the inelastic component could not be analyzed reliably for $E \leq 2\,\text{meV}$.

An overall softening of the phonon spectrum is observed when cooling from $300\,\text{K}$ to $10\,\text{K}$. This is contrary to what is expected, that is, a stiffer lattice yielding larger phonon frequencies. However, an enhancement of the electronic density of states at the Fermi level upon cooling can damp lattice vibrations in systems where EPC is important, as has been observed, for example, in Nb and $\text{YNi}_2\text{B}_2\text{C}$ [25, 26]. In particular, the $10\,\text{K}$ data shows a pronounced increase of spectral weight below $10\,\text{meV}$ with respect to the room-temperature data, in agreement with the enhanced line broadening and the strong coupling of these low-energy phonons to the electronic system predicted by the DFPT calculations.

To compare the experimental results with the predictions of the DFPT, calculations of inelastic powder spectra including experimental and EPC (from DFT calculations) line-broadening are presented in Fig. 2(a) as green (no SOC) and red (with SOC) lines [27]. The calculations match fairly well the energy and relative intensity of the peaks of the experimental data above $7\,\text{meV}$. How-
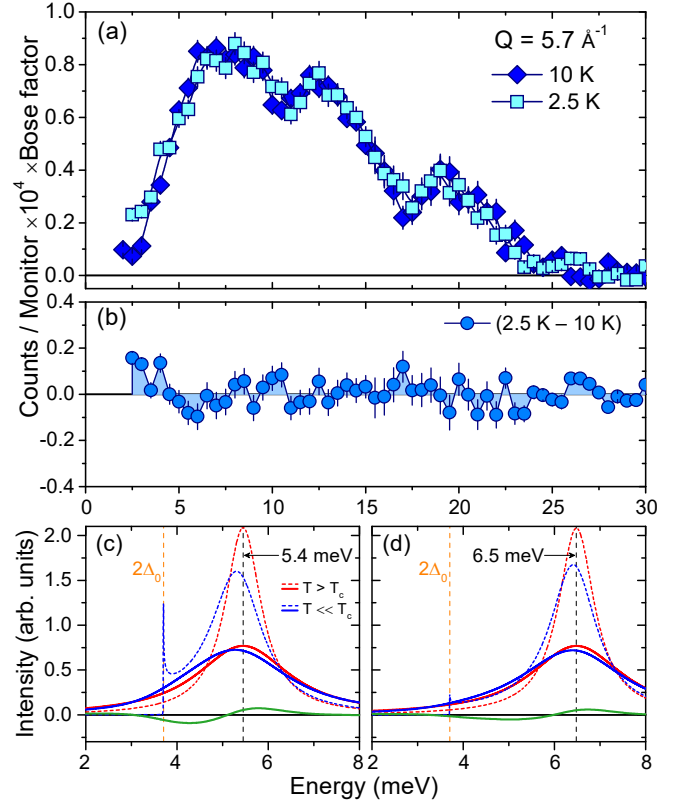

FIG. 3: (color online). (a) Inelastic data from combined energy scans at $Q = 5.7\,\text{Å}^{-1}$ obtained above (diamonds) and below (squares) T_c. The difference between these spectra is displayed in (b). (c-d) Example of calculations of phonon line shapes based on the theory of Allen et al. [24] for the first optic phonon mode at the Γ point for a single crystal. Red and blue curves correspond to temperatures above and below T_c, respectively. The broadening of the dashed curves is due only to the EPC effect presented in Fig. 1(c), while for the solid lines, an additional instrumental broadening is also included (see text).

ever, there is a strong discrepancy between experiment and theory at lower energies. First, the position of the calculated low-energy phonon band lies about $1.7\,\text{meV}$ below the lowest measured peak. Second, the amplitude of the calculated phonon powder spectra differs from the experimental data particularly at low energies. The inclusion of SOC enhances the EPC and further softens the powder spectrum (red line), leading to a slightly smaller amplitude. Still, the inclusion of SOC in the calculations does not provide a good agreement with the experimental measurement.

We conclude that the DFPT calculations underestimate the energy of the lowest band of phonon modes indicating that the coupling of these modes to the electronic subsystem is overestimated. If the calculations were adjusted to increase the energy of this phonon band, then this would result automatically in a decrease in the strength of the estimated EPC. In order to simulate the

impact of such a shift on the EPC and superconducting properties, we artificially scaled the Eliashberg function by shifting $\omega_{sh} = \omega + 1.7\,\text{meV}$ in an energy range up to $6.2\,\text{meV}$. The resulting scaled Eliashberg function $\alpha^2 F(\omega_{sh}) = (\omega/\omega_{sh})\,\alpha^2 F(\omega)$ is presented in Fig. 2(c). This procedure yields a reduction of the EPC parameter λ from 1.97 to 1.24, corresponding to an estimated $T_c = 8\,\text{K}$ for $\mu^* = 0.1$, in good agreement with the experiment.

Upon entering the superconducting state, a change in the phonon spectra at energies near $2\Delta(T)$ is expected to occur in systems presenting strong EPC [24, 28], because the number of possible excited electronic states by a phonon is zero for energies smaller than 2Δ. Fig. 3(a) displays the combined spectra collected above $(10\,\text{K})$ and below $(2.5\,\text{K})$ T_c and, in (b), their difference. The inelastic data show no clear change between the two measurements at low energies near $2\Delta_0 \sim 3.7\,\text{meV}$ within statistical error. The calculations of phonon line shapes based on the theory of Allen *et al.* [24] are presented in Fig. 3(c) and (d) for the single-crystalline case, and suggest two effects that are detrimental to the experimental observation of a change in the phonon spectrum below T_c in our measurements. First, in Fig. 3(c), a phonon peak at $5.4\,\text{meV}$ (dashed red line), as predicted by DFPT at the Γ point with a FWHM of $1\,\text{meV}$ due to EPC, would soften and develop a sharp anomaly near $E = 2\Delta_0$ for $T \ll T_c$ (dashed blue line). When one considers the experimental resolution (solid red and blue lines, pseudo-Voight line shape with a FWHM of $1.55\,\text{meV}$ and 80% Lorentzian weight), only a mild softening would be noticeable at low temperatures, resulting in a small difference between the curves above and below T_c (green line). Second, a phonon peak shifted to higher energies as it is found in the IXS data would make the effect even smaller, as shown in Fig. 3(d). The effect below T_c is expected to be less prominent in the powder experiments due to Q-space averaging and to the larger background arising from incoherent scattering at these lower energy transfers.

In summary, we presented IXS experiments performed on powder samples of SrPt$_3$P. The room-temperature phonon spectrum shifts towards lower energies upon cooling, which can be understood in terms of a damping of lattice vibrations due to strong EPC and the enhanced electronic density of states near the Fermi level at low temperatures. A strong EPC is predicted by our calculations, in close agreement with previously reported results. The inclusion of SOC due to the presence of Pt-5d states yields a large EPC coupling constant $\lambda \sim 2$. However, when comparing the experimental and theoretical data with and without SOC, we conclude that theoretical models overestimate the coupling of the low-energy phonon modes to the electronic system. Adjusted EPC parameters reproduce the experimentally observed T_c fairly well. Further experiments should be performed, if possible, in currently unavailable single crystals, to explore the low-energy phonon spectrum with regard to the intrinsic phonon linewidths as well as the superconductivity-induced changes of the line shape.

———

* Corresponding author: diego.zocco@kit.edu
† Corresponding author: frank.weber@kit.edu

[1] D. N. Basov and A. V. Chubukov, Nat. Phys. **7**, 272 (2011).
[2] J. Nagamatsu, N. Nakagawa, T. Muranaka, T. Zenitani, and J. Akimitsu, Nature **410**, 63 (2001).
[3] N. W. Ashcroft, Phys. Rev. Lett. **92**, 187002 (2004).
[4] A. P. Drozdov, M. I. Eremets, I. A. Troyan, V. Ksenofontov, and S. I. Shylin, arXiv:1506.08190 (2015).
[5] T. Takayama, K. Kuwano, D. Hirai, Y. Katsura, A. Yamamoto, and H. Takagi, Phys. Rev. Lett. **108**, 237001 (2012).
[6] R. Khasanov, A. Amato, P. K. Biswas, H. Luetkens, N. D. Zhigadlo, and B. Batlogg, Phys. Rev. B **90**, 140507 (2014).
[7] I. A. Nekrasov and M. V. Sadovskii, JETP Letters **96**, 227 (2012).
[8] H. Chen, X. Xu, C. Cao, and J. Dai, Phys. Rev. B **86**, 125116 (2012).
[9] C.-J. Kang, K.-H. Ahn, K.-W. Lee, and B. Il Min, J. Phys. Soc. Jpn. **82**, 053703 (2013).
[10] A. Subedi, L. Ortenzi, and L. Boeri, Phys. Rev. B **87**, 144504 (2013).
[11] S. G. Louie, K.-M. Ho, and M. L. Cohen, Phys. Rev. B **19**, 1774 (1979).
[12] B. Meyer, C. Elsässer, and M. Fähnle, *FORTRAN90 Program for Mixed Basis Pseudopotential Calculations for Crystals* (Max-Planck-Institut für Metallforschung, Stuttgart, unpublished).
[13] J. P. Perdew and Y. Wang, Phys. Rev. B **45**, 13244 (1992).
[14] D. Vanderbilt, Phys. Rev. B **32**, 8412 (1985).
[15] L. Kleinman, Phys. Rev. B **21**, 2630 (1980).
[16] G. B. Bachelet and M. Schlüter, Phys. Rev. B **25**, 2103 (1982).
[17] R. Heid, K.-P. Bohnen, I. Y. Sklyadneva, and E. V. Chulkov, Phys. Rev. B **81**, 174527 (2010).
[18] C. L. Fu and K. M. Ho, Phys. Rev. B **28**, 5480 (1983).
[19] Due to the large couplings, phonon frequencies and EPC exhibited a strong dependence on the applied broadening and the density of the k mesh. Sufficient convergence was obtained with a $12 \times 12 \times 12$ k mesh for the phonon dispersion, and a $16 \times 16 \times 16$ k mesh for the calculation of the EPC properties. Phonon and EPC properties were determined via DFPT on a $4 \times 4 \times 4$ q-point mesh including contributions from SOC.[17] These results were then interpolated for arbitrary q points using Fourier techniques to accurately determine the Eliashberg function. Superconducting properties were analyzed by solving the isotropic Eliashberg gap equations.
[20] S. Baroni, S. de Gironcoli, A. Dal Corso, and P. Giannozzi, Rev. Mod. Phys. **73**, 515 (2001).
[21] R. Heid and K.-P. Bohnen, Phys. Rev. B **60**, R3709

(1999).

[22] P. B. Allen, Phys. Rev. B **6**, 2577 (1972).

[23] Typical counting times varied from 60 to 120 seconds using 0.5 meV energy steps. Diffraction scans (2θ) were performed before measurements to determine the position of incoherent elastic peaks. The energy scans displayed in Figs. 2 and 2 correspond to the selected angle of $\sim 30°$ ($Q = 5.7\,\text{Å}^{-1}$) with low number of elastic counts, which matched the position of one of the instrument's analyzers.

[24] P. B. Allen, V. N. Kostur, N. Takesue, and G. Shirane, Phys. Rev. B **56**, 5552 (1997).

[25] N. Wakabayashi, Phys. Rev. B **33**, 6771 (1986).

[26] F. Weber, L. Pintschovius, W. Reichardt, R. Heid, K.-P. Bohnen, A. Kreyssig, D. Reznik, and K. Hradil, Phys. Rev. B **89**, 104503 (2014).

[27] Phonon structure factors (PSF) were calculated for a single crystal of $SrPt_3P$, including the experimental resolution, for a total of 853 Brillouin zones with scattering vectors of absolute value $Q \leq 12\,\text{Å}^{-1}$ in the first octant of the reciprocal space and for the respective 8000 reduced wavevectors. To account for the $1/\omega$-dependence of the phonon intensity, the PSF have been weighted in accordance with the relevant phonon energy. For the powder averaging, the individual PSF were summed within spherical shells $Q + dQ$. Due to the quadratic increasing number of Q-points, the Q^2-dependence for the powder spectrum in this summation is implied.

[28] F. Weber, A. Kreyssig, L. Pintschovius, R. Heid, W. Reichardt, D. Reznik, O. Stockert, and K. Hradil, Phys. Rev. Lett. **101**, 237002 (2008).